

1 **Sea surface temperature variability in the Norwegian Sea during the**
2 **late Pliocene linked to subpolar gyre strength and radiative forcing**

3 Paul E. Bachem^{a*}, Bjørg Risebrobakken^a, Erin L. McClymont^b

4 ^a Uni Research Climate, Bjerknes Centre for Climate Research, NO-5007 Bergen, Norway

5 ^b Department of Geography, Durham University, Durham DH1 3LE, UK

6

7 * Corresponding author. Uni Research Climate, Nygårdsgaten 112, NO-5007 Bergen, Norway.

8 Tel.: +47 55589870. E-mail address: paul.bachem@uni.no

9

10

11 Keywords: Pliocene, Norwegian Sea, ODP Site 642, alkenones, SST, subpolar gyre

12

13

14

15

16

17

18

19 **Abstract**

20 The mid-Piacenzian warm period (3.264-3.025 Ma) of the Pliocene epoch has been proposed as a
21 possible reference for future warm climate states. However, significant disagreement over the
22 magnitude of high latitude warming occurs between data and models at this time, raising questions
23 about the driving mechanisms and feedbacks which were responsible. We have developed a new set
24 of orbital-resolution alkenone-based sea surface temperature (SST) and ice rafted debris (IRD)
25 records from the Norwegian Sea spanning 3.264-3.14 Ma. The SSTs in the Norwegian Sea were 2-
26 3°C warmer than the Holocene average, likely caused by the radiative effect of higher atmospheric
27 CO₂ concentrations. There is notable obliquity-driven SST variability with a range of 4°C, shown by
28 evolutive spectra. The correlation of SST variability with the presence of IRD suggests a common
29 climate forcing acting across the Nordic Seas region. Changes of the SST gradient between the
30 Norwegian Sea and North Atlantic sites suggest that the subpolar gyre was at least as strong as
31 during the Holocene, and that the northward heat transport by the North Atlantic Current was
32 comparable.

33

34

35

36

37

38

39

40

41

42 **1. Introduction**

43 The mid-Piacenzian is known to be globally warmer than today, based on both proxy
44 reconstructions and model simulations (Dowsett et al., 2013a; Haywood et al., 2013a). Throughout
45 geological history, high latitude regions show enhanced environmental changes because of stronger
46 feedback mechanisms, such as the ice-albedo feedback, the amount of Arctic sea ice, vegetation and
47 freshwater balance (Miller et al., 2010). Prescott et al. (2014), using HadCM3 and applying varying
48 orbital forcing, found significant differences between the mid-Piacenzian interglacials of Marine
49 Isotope Stage (MIS) KM5 and KM1. These results show that the climate variability of the mid-
50 Piacenzian needs to be examined closer if model-data comparisons are to become more informative.

51 In the Nordic Seas the available proxy data disagree with results from climate model simulations on
52 mid-Piacenzian sea surface temperatures (SSTs): much larger warm anomalies appear in the proxy
53 data (Robinson, 2009) than in most of the models that were used in the Pliocene Model
54 Intercomparison Project (PlioMIP) (Haywood et al., 2013a). One reason for this data-model
55 mismatch is the comparison of long-term averaged proxy data over a 239 ka interval (ca. 3.264-
56 3.025 Ma, Dowsett et al., 2010) with model integrations that represent one focused but shorter
57 interval in time (Haywood et al., 2013b). A further problem is the low amount of high latitude sites
58 from which data stems. Planned modelling projects aim to utilize information from new Norwegian
59 Sea data (Haywood et al., 2015). Furthermore, the PlioMIP boundary conditions were so far based
60 on the assumption that the mid-Piacenzian had largely modern paleogeographic features. However,
61 using the HadCM3 model, Hill (2015) found stronger warming in the northern Nordic Seas by
62 introducing a deeper Greenland-Scotland Ridge, a subaerial Barents Sea, and a changed pattern of
63 river runoff at high northern latitudes. Hence, knowing how the paleogeographic boundary

64 conditions differed from the present, and the climatic effects of these differences, is important for
65 understanding the mid-Piacenzian climate and to resolve model-data inconsistencies.

66 Existing data from the Nordic Seas show a broad range of SSTs. In the northern Nordic Seas, SSTs
67 as warm as 10.5 to 19.3°C, which is 9 to 18°C above modern summer temperatures, have been
68 reported between 3.3 and 3 Ma (Boyer et al., 2013; Robinson, 2009). These SSTs were based on the
69 $U^{K'}_{37}$ alkenone index and Mg/Ca of foraminifera. In contrast, SSTs of 4-5°C are reported for the
70 mid-Piacenzian for the same region based on archaea biomarkers (Knies et al., 2014b). The large
71 discrepancies between the reconstructions emphasize the unknowns of the temperature development
72 of this region. At the Iceland Plateau, in the central Nordic Seas, mid-Piacenzian SSTs of 8.5-12.3°C
73 (3.4-7.2°C above modern summer SSTs) are indicated using the Mg/Ca and $U^{K'}_{37}$ proxies
74 (Robinson, 2009; Schreck et al., 2013). So far no mid-Piacenzian SST data has been available from
75 the Norwegian Sea (Dowsett et al., 2013a).

76 Despite the range of reported SSTs for the mid-Piacenzian Nordic Seas, a clear signal of a region
77 which was warmer than modern emerges in both data and in models (Dowsett et al., 2010; Haywood
78 et al., 2013a). In contrast, the occurrence of mid-Piacenzian Ice Rafted Debris (IRD) indicates that
79 icebergs were occasionally moving into the region (Jansen et al., 2000), even though icebergs are
80 rarely seen in the Norwegian Sea today. Low amounts of IRD are, however, also seen in the
81 Norwegian Sea during the Holocene (Moros et al., 2004). This suggests that a low background IRD
82 input is not unusual for this region during warm climate phases. Greenland, Iceland and Scandinavia
83 have been discussed as source regions of Pliocene icebergs in the Nordic Seas (Jansen et al., 2000).
84 Such icebergs would have to originate from terrestrial glaciers with connections to the sea, but the
85 initial timing and nature of the Northern Hemisphere Glaciation (NHG) is still poorly understood.
86 Proxy data show that major thresholds in the development towards stronger glaciation were crossed

87 near 3.6 Ma and 2.7 Ma (Kleiven et al., 2002; Lisiecki and Raymo, 2005; Mudelsee and Raymo,
88 2005; Naafs et al., 2012). Several factors have been suggested as influential for the climate
89 progression up to this threshold, such as decreasing atmospheric CO₂ (Lunt et al., 2008), extremes in
90 orbital forcing (Maslin et al., 1998), and topographic shifts or closures of seaways that lead to
91 changes in ocean currents and northward heat transport (e.g. Haug and Tiedemann, 1998; Schepper
92 et al., 2015).

93 The Nordic Seas and the North Atlantic are tightly connected through the ocean circulation of the
94 North Atlantic Current (NAC), Norwegian Atlantic Current (NwAC) and East Greenland Current
95 (EGC) (Hansen and Østerhus, 2000). In the subpolar gyre of the North Atlantic, mid-Piacenzian
96 SSTs were on average 6.3°C higher than the modern summer mean (Lawrence et al., 2009; ODP
97 Site 982). In the northern boundary of the North Atlantic subtropical gyre they were 2-3°C higher
98 (Naafs et al., 2010; IODP Site U1313). Both records have a high enough temporal resolution to
99 show orbital scale variability and temperature trends through the mid-Piacenzian. Due to the lack of
100 data from the Norwegian Sea, and differing temporal resolution in available reconstructions from
101 the Nordic Seas and the North Atlantic, the links between the North Atlantic and the Nordic Seas,
102 and hence variations in northward heat transport to the Arctic, are not well known.

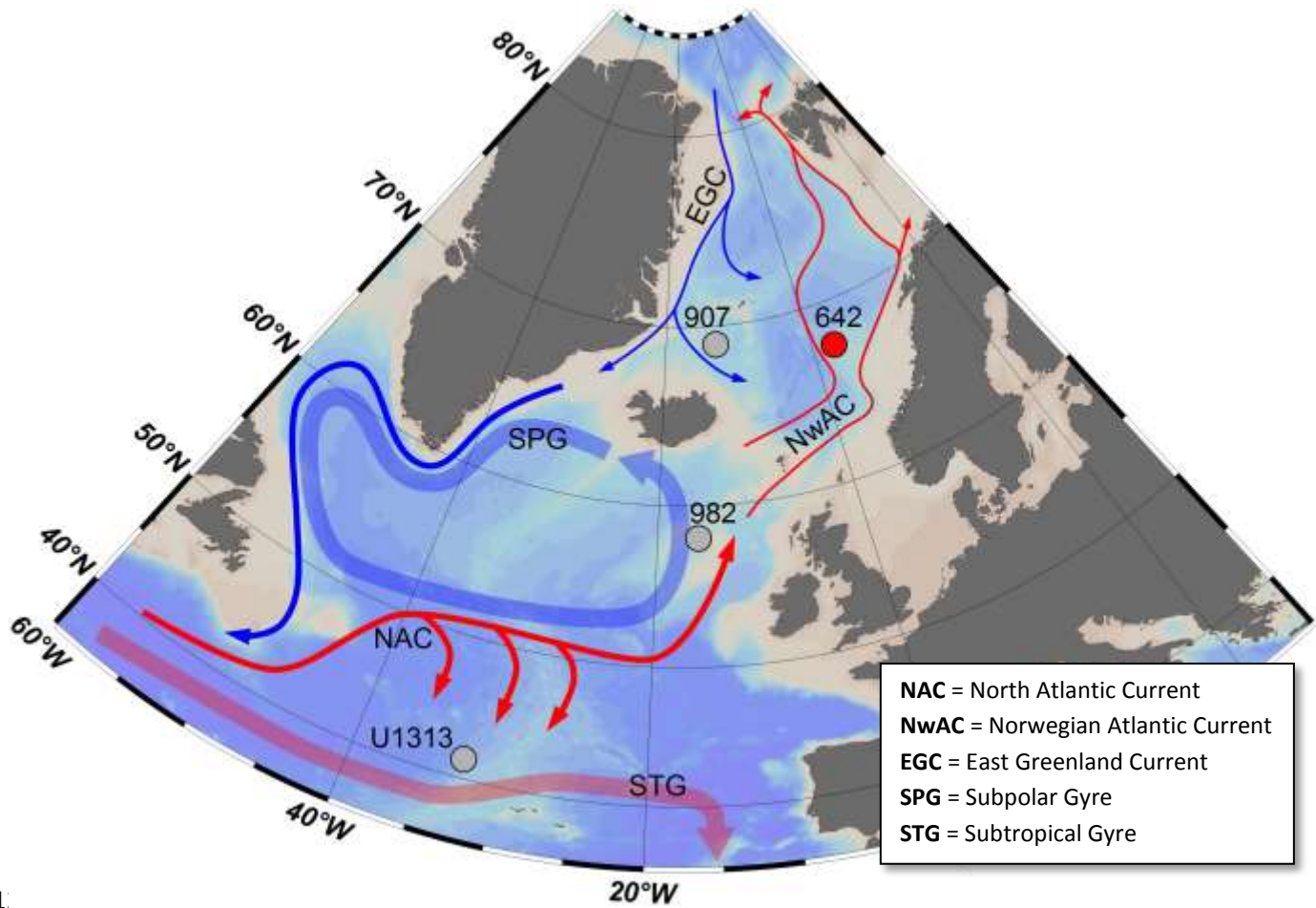
103 In order to improve on this situation, we aim to 1) determine the average SST of the Norwegian Sea
104 during the mid-Piacenzian, 2) determine the magnitude and variability of SST changes over orbital
105 time scales, 3) assess which climate factors were most likely affecting the Norwegian Sea, and 4)
106 investigate the relationship between SSTs in the Norwegian Sea and the North Atlantic. To address
107 these aims we present a new mid-Piacenzian Norwegian Sea SST dataset based on the U^K₃₇
108 alkenone index. Using new high-resolution IRD counts we correlate the variability of early Northern
109 Hemisphere Glaciation with the variability of Norwegian Sea SSTs. Lastly, we discuss the mid-

110 Piacenzian meridional SST gradient between the Norwegian Sea and the North Atlantic to estimate
111 the influence of the NAC on the Nordic Seas.

112

113 **2. Regional Setting**

114 The subpolar gyre of the North Atlantic is a counterclockwise surface circulation between Iceland,
115 Greenland and Northern Canada that is driven by buoyancy differences, inflowing waters of the
116 EGC and the regional wind system. The subtropical gyre is a largely wind-driven clockwise surface
117 circulation in the North Atlantic between 40°N and 15°N. The NAC transports water north- and
118 eastward between these two gyres, leading to mixing of water from both gyres south of Iceland, with
119 the subpolar gyre acting as a regulator of the inflow of Atlantic Water into the Norwegian Sea. (Fig.
120 1) (Hátún et al., 2005).



1..

122 **Figure 1:** Modern circulation of the North Atlantic and Nordic Seas (based on Blindheim and Østerhus, 2005; Hátún et
 123 al., 2005). Relatively warmer currents are marked in red, colder ones in blue. The subtropical gyre and the subpolar gyre
 124 are marked in lighter red and blue respectively. ODP Site 642, studied in this paper, is marked with a red dot; other
 125 discussed sites are marked with gray dots. The map was generated using Ocean Data View (Schlitzer, 2015).

126

127 The Nordic Seas, consisting of the Greenland Sea, Iceland Sea and Norwegian Sea, are a relatively
 128 small but oceanographically complex region situated between Iceland, Greenland and Norway. The
 129 main flow of water into the Nordic Seas takes place across the eastern part of the Greenland-
 130 Scotland Ridge, specifically over the Iceland-Faroe Ridge and the Faroe-Shetland Channel, with a
 131 combined northward inflow of 7 Sv (1 Sverdrup = $10^6 \text{ m}^3/\text{s}$) (Blindheim and Østerhus, 2005). The

132 Norwegian Atlantic Current (NwAC) transports warm and saline (9-10.5°C, 34.4-34.7 psu,
133 Blindheim and Østerhus, 2005) Atlantic water along the slope northward into the Norwegian Sea,
134 where it continuously cools through interaction with the atmosphere. A fraction of the water mass
135 flows eastward of northern Norway into the Barents Sea, from where a branch continues through the
136 Arctic Ocean. At the Fram Strait, the main gateway for northern in- and outflow of water masses a
137 net southward flow in the order of 2-6 Sv forms the East Greenland Current (EGC). The coastal
138 portion of the EGC is made up of 1 Sv of Polar water which is formed in the Arctic Ocean.
139 Alongside Arctic intermediate and deep water masses, two altered forms of Atlantic water join the
140 EGC. One type consists of Atlantic water branching westward in the West Spitsbergen Current, the
141 second enters the Arctic Ocean, traverses through it and joins the EGC through the western Fram
142 Strait. Flowing towards the Denmark Strait, the EGC entrains Greenland Sea Water which forms
143 through convection of deep and intermediate water in the Greenland Sea (Blindheim and Østerhus,
144 2005). Aside from the surface flow of the EGC of 1.3 Sv, most southward outflow from the Nordic
145 Seas occurs over the deepest parts of the Greenland-Scotland Ridge, with about 3 Sv each flowing
146 over the Denmark Strait sill and over the Iceland-Scotland Ridge. The current system of the Nordic
147 Seas sets up strong east-west temperature and salinity gradients between Atlantic Water in the east
148 and Polar Water in the west. Atlantic and Polar water mix in the central Nordic Seas through gyres
149 branching off from the EGC into the Greenland Sea and the Iceland Sea. The water mass in the
150 mixing zone is referred to as Arctic water.

151

152 **3. Material and Methods**

153 **3.1 Samples and age model**

154 The study site, Ocean Drilling Program (ODP) Hole 642B (Leg 104), is located on the outer Vøring
155 Plateau, at 67°13.5'N, 2°55.7'E in 1286 m water depth, 400 km off the Norwegian coast (Fig. 1).

156 The sea floor at this site lies underneath the western branch of the NwAC. For this study the core
157 was analyzed in 1 cm steps between 66.99 and 68.39 meters below sea floor (mbsf). A lack of core
158 material precluded sampling between 67.89 and 68.03 mbsf.

159 The age model of Hole 642B is based on an updated paleomagnetism record and a correlation of a
160 benthic $\delta^{18}\text{O}$ record for this site with the LR04 stack (Fig. 2g; Risebrobakken et al., in review;
161 Lisiecki and Raymo, 2005). The resulting sedimentation rate is between 0.23 and 1.83 cm/ka, with
162 an average of 1.17 cm/ka.

163 A hiatus exists in the Hole 642B sediment record at ca. 3.1 Ma (Jansen and Sjøholm, 1991). We end
164 our record at the 3.14 Ma (66.99 mbsf) position due to strongly increased coarse fraction content in
165 younger samples. This coarse material could indicate lag deposits, marking an erosional hiatus.

166 While the benthic $\delta^{18}\text{O}$ record from Hole 642B in general matches the global benthic $\delta^{18}\text{O}$ LR04
167 stack well, the absolute amplitude of the Marine Isotope Stage (MIS) M2 signal is small relative to
168 the global and North Atlantic signals (De Schepper et al., 2013; Lisiecki and Raymo, 2005,
169 Risebrobakken et al., in review). Together with a lack of IRD input compared to the pronounced
170 IRD peaks at the Iceland Plateau (Jansen and Sjøholm, 1991), the relatively weak benthic $\delta^{18}\text{O}$
171 signal through the peak of MIS M2 hints at the possibility of a minor hiatus at Hole 642B. Our study
172 focuses on the time period between the beginning of MIS M1 and the later Pliocene hiatus (from
173 3.264 Ma to 3.14; 68.07 mbsf to 66.99 mbsf). This time interval includes the time slice proposed by
174 Haywood et al. (2013b), which is centered on 3.205 Ma.

175 **3.2 Ice Rafted Debris**

176 Mineral grains above 63 μm in size that are found in marine sediments have been transported from
177 their terrestrial origins by moving ice, as they are too heavy to be transported by wind (e.g. Jansen et
178 al., 2000). A previous study of IRD was conducted at Hole 642B on the >125 μm sediment fraction
179 with samples taken in 3-19 cm steps (Jansen and Sjøholm, 1991). In our study we visually inspected
180 the >150 μm fraction at 1 cm steps, significantly increasing the resolution compared to Jansen and
181 Sjøholm (1991). While this approach misses the IRD of smaller grain sizes, the >150 μm IRD
182 fraction suffices to correlate the presence and variability of IRD in the Nordic Seas region to SSTs.
183 All grains of ascertained terrestrial origin as based on their mineralogy were counted as IRD. The
184 results are presented as number of grains per gram of dry sediment.

185 **3.3 Alkenone UK'_{37} Index**

186 Alkenone measurements were carried out on 77 samples at the biomarker laboratory of the
187 Department of Geography at Durham University, UK. For these measurements, samples of 1 to 2 g
188 sediment were freeze-dried and homogenized with an agate mortar and pestle. Lipids were extracted
189 using a CEM MARS microwave following the protocol of Kornilova and Rosell-Melé (2003). For
190 this process, 12 ml of Dichloromethane (DCM) and Methanol (3:1 v/v) were added to the samples,
191 with a known quantity of the internal standard 2-nonadecanone (Sigma-Aldrich). The microwave
192 temperature was ramped up to 70°C over 2 minutes, held there for 5 minutes, and allowed to cool
193 down to <30°C before further processing. The sediment residue was removed by centrifugation, and
194 the lipid extracts dried with a rotary evaporator. Alkenones were isolated from the total extract using
195 silica column chromatography, eluting with *n*-hexane (for apolar compounds), DCM (for ketones)
196 and methanol (for polar compounds). The ketone (alkenone) fractions were dried under N_2 and
197 stored below 4°C until further analysis.

198 Alkenones were quantified with a Thermo Scientific Trace 1310 gas-chromatograph (GC) fitted
199 with a flame ionization detector (FID) and a Restek Rxi-5ms fused silica column (30m length,
200 0.25mm internal diameter, low polarity crossbond diphenyl dimethyl polysiloxane phase). Hydrogen
201 was used as the carrier gas with a constant flow rate of 1.7 ml/min. The injector temperature was set
202 to 280°C, FID temperature to 350°C. After injection, the oven temperature was held at 70°C for 3
203 minutes, increased at 12°C/min to 170°C, then at 6°C/min to 310°C and held for 40 minutes.

204 The $U_{37}^{K'}$ index was calculated according to Prahl and Wakeham (1987):

205
$$U_{37}^{K'} = \frac{[C_{37:2}]}{[C_{37:2}] + [C_{37:3}]}$$

206 The global core-top calibration of Müller et al. (1998) was used to reconstruct temperature (T)
207 values from the $U_{37}^{K'}$ index:

208
$$U_{37}^{K'} = 0.033 \times T + 0.044$$

209 The calibration has an uncertainty of $\pm 1^\circ\text{C}$.

210

211 **4. Results**

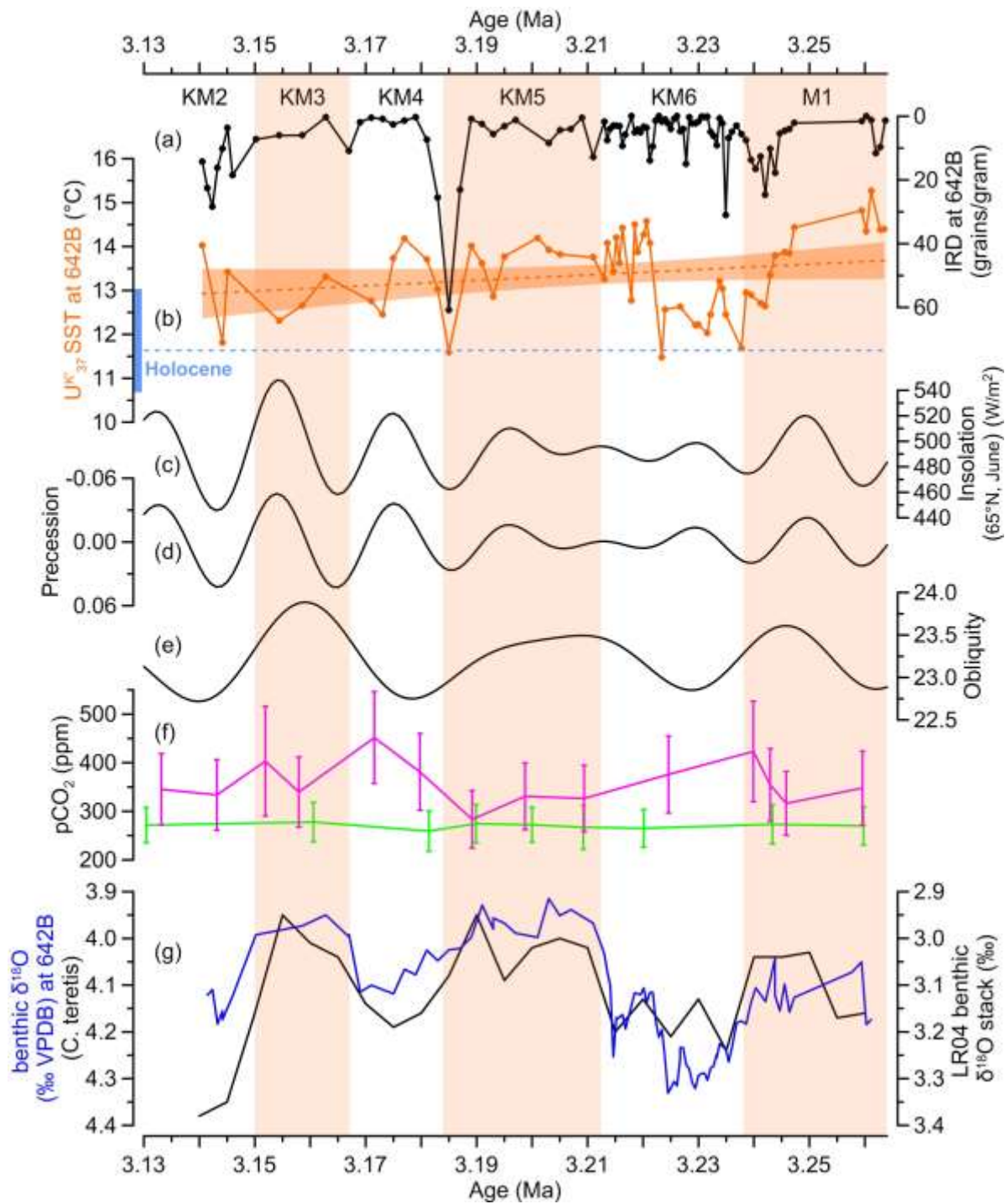
212 The Hole 642B SST and IRD records cover the 3.264-3.14 Ma (68.07-66.99 mbsf) time window
213 (Fig. 2b,c). Measurable amounts of alkenones were obtained from 59 samples within this interval.
214 Their $U_{37}^{K'}$ index ranges between 0.42 and 0.55, resulting in an SST range of 11.5°C-15.6°C, with
215 an average of 13.4°C, using the Müller et al. (1998) calibration. A slight cooling trend of 0.7°C per
216 100 ka takes place over the whole time interval. However, this trend is not significant within the
217 95% confidence interval and is smaller than the ca. 1°C uncertainty of the calibration. While there is

218 no robust long-term trend, the SSTs vary on orbital time scales. A cooling from 15°C to 11.5°C
219 takes place throughout MIS M1 and the first half of MIS KM6. Subsequently, SSTs increase to
220 14.5°C over a few ka in the middle of MIS KM6 (3.225-3.220 Ma, 67.54-67.45 mbsf). A slower
221 overall cooling from 14.5-11.8°C takes place from 3.22 to 3.144 Ma (67.45-67.04 mbsf). A more
222 pronounced short-term cooling to 11.5°C occurs at 3.185 Ma (67.20 mbsf), at the MIS KM5/KM4
223 transition.

224 For IRD analysis 94 samples were available. Their IRD content varies between 0 and 60 grains per
225 gram of sediment, with an average of 6.2 grain/g. In the early part of MIS M1, IRD counts are
226 around 2-10 grains/g. An increase of IRD to 25 grains/g is recorded towards the end of MIS M1.
227 The IRD amount is variable in MIS KM6, between 0 and 30 grains/g. The largest IRD amount of 60
228 grains/g is reached at the end of KM5. Another increase in IRD to 28 grains/g appears in KM2.

229 Sea surface temperatures and IRD covary. Elevated IRD content occurs during periods of cooling.
230 The highest IRD peaks are found at 3.24 Ma, 3.185 Ma and at 3.145 Ma, coinciding with some of
231 the lowest recorded SSTs.

232



233

234 **Figure 2:** (a) IRD per gram of sediment from 642B; (b) SSTs based on the U^{K}_{37} index (Müller et al., 1998 calibration)
 235 from 642B. The orange dashed line marks the linear trend; the orange shaded area indicates its 95% confidence interval.
 236 The light blue dashed line shows the Holocene mean SST from Site MD95-2011. The vertical light blue line on the left
 237 indicates the full range of Holocene SSTs (Calvo et al., 2002); (c) daily mean June insolation at 65°N; (d) precession; (e)

238 obliquity (c-e from Laskar et al., 2004); (f) atmospheric CO₂ concentrations (green, Badger et al., 2013; magenta,
239 Martínez-Botí et al., 2015); (g) benthic stable oxygen isotopes from Hole 642B (Risebrobakken et al., in review)
240 compared to the LR04 stack (Lisiecki and Raymo, 2005). Orange vertical bars indicate MIS based on Lisiecki and
241 Raymo (2005).

242

243 **5. Discussion**

244 **5.1 Environmental interpretation of the alkenone proxy in the Norwegian Sea**

245 Our results indicate that mid-Piacenzian Norwegian Sea U^{K'}₃₇ SSTs were on average 5.5°C warmer
246 than the recent annual mean temperature (1955-2012), 3°C warmer than local modern summer
247 temperature (1955-2012, JAS, Boyer et al., 2013), and 2°C warmer than the Holocene mean U^{K'}₃₇
248 SSTs in the same area (Calvo et al., 2002). The main growth period of modern alkenone producing
249 organisms in high latitudes are the summer months, due to low solar input in the winter (Andrulleit,
250 1997). While the calibration equation of Müller et al. (1998) is defined for annual mean
251 temperatures up to 60°N, when it is applied to Holocene sediments in the Nordic Seas, at higher
252 latitudes, the results more closely reflect summer temperatures (Risebrobakken et al., 2011, 2010).
253 Therefore, comparing our alkenone-based proxy data to summer temperatures is more appropriate
254 than comparing them to modern annual mean temperatures. However, since our study interval
255 covers 123 ka of a warm climate, and each measurement represents an averaging of 0.5-4 ka, the
256 short instrumental interval is not an ideal comparison. Furthermore, the instrumental data is already
257 influenced by human activities (e.g. Stocker et al., 2013), and are not representative of natural
258 climate variability. The Holocene mean U^{K'}₃₇ SSTs from nearby Site MD95-2011 (Calvo et al.,
259 2002) include the range of summer temperature variability (10.6-13.0°C, Fig. 2b) that existed within
260 a warm interglacial climate. For these reasons we discuss the mid-Piacenzian U^{K'}₃₇ SSTs and their
261 variability relative to this Holocene mean (Fig. 2b, dashed line). The mean annual SSTs of the mid-

262 Piacenzian should be expected to be lower than our measured SSTs, same as in the modern-day and
263 during the Holocene.

264 **5.2 Causes of mid-Piacenzian Norwegian Sea SST warmth and long-term stability**

265 The mid-Piacenzian SSTs were 2°C warmer than the Holocene SSTs in the Norwegian Sea (Fig. 2).
266 These warmer SSTs may be caused by a range of factors. Here, we discuss the relation of SSTs to
267 the atmospheric CO₂ concentrations, to northward heat transport by the NAC, to lower ice-albedo
268 feedback due to lack of widespread northern hemisphere glaciation, and to geographic differences
269 between the Pliocene and the present.

270 At a global scale, higher (lower) greenhouse gas concentrations are tightly linked to higher (lower)
271 temperatures, but constraining the magnitude of the temperature response through time and on
272 regional scales is complicated by uncertainties around a number of climate feedbacks including ice
273 sheet albedo and sea ice extent (e.g. Martinez-Boti et al., 2015). Mid-Piacenzian atmospheric CO₂
274 values range between the Holocene mean (ca. 270 ppmv, e.g. Indermühle et al., 1999) and modern-
275 day values (ca. 400 ppmv) (Badger et al., 2013b; Martínez-Botí et al., 2015). Distinct differences
276 between reconstructions based on different methods make it difficult to pinpoint a mean
277 concentration and variability of CO₂ for the Piacenzian. Badger et al. (2013b) show stable
278 atmospheric CO₂ around the Holocene mean based on $\delta^{13}\text{C}$ of alkenones, while Martinez-Boti et al.
279 (2015) published a record based on boron isotopes with higher CO₂ mean and increased variability
280 (Fig. 2f). Despite the differences between various reconstructions, most agree on higher than
281 Holocene CO₂ concentrations during the mid-Piacenzian (Martínez-Botí et al., 2015). The warmth
282 seen in the 642B SST record could at least in part be explained by the increased radiative forcing
283 caused by higher concentrations of atmospheric CO₂. The importance of CO₂ for Pliocene climate
284 development is emphasized in model simulations by Lunt et al. (2008), suggesting that decreasing

285 atmospheric CO₂ was critical for an increase in northern hemisphere glaciation and cooling during
286 the late Pliocene.

287 Increased northward heat transport by the NAC due to a stronger overturning circulation has been
288 proposed as a driver of warm mid-Piacenzian climate (Raymo et al., 1996). Since the NwAC is
289 closely linked to the NAC (Fig. 1), this could explain the generally higher SSTs at Hole 642B.
290 However, other studies have shown that there is no direct coupling between heat transport and
291 overturning strength, which indicates that increased northward heat transport is not necessarily a
292 factor in mid-Piacenzian warmth (Haywood & Valdes, 2004; Zhang et al., 2013; Hill, 2015).

293 Haywood and Valdes (2004) emphasize the difference in ice-albedo feedback between the Pliocene
294 and the present as an essential mechanism for the different past and modern high latitude
295 temperature regimes. Less energy would be reflected in the northern hemisphere during the mid-
296 Piacenzian due to a lower ice-albedo feedback as a result of a smaller sea ice cover and the lack of
297 large-scale glaciation on the northern hemisphere. Our record shows that the average SST in the
298 Norwegian Sea was not significantly higher than the global average warmth modeled in mid-
299 Piacenzian simulations (Haywood and Valdes, 2004, SAT; Haywood et al., 2013a; SAT-MMM).
300 Thus the Norwegian Sea does not, on average, reflect a strong influence of the ice-albedo feedback.
301 This is expected, since there is no notable influence of the ice-albedo feedback in the Norwegian Sea
302 in the modern climate. However, it is possible that atmospheric dynamic feedbacks related to
303 smaller ice sheets and sea ice played a role in the northern hemisphere climate system (e.g. Khodri
304 et al., 2005).

305 Differences in geographic boundary conditions may also have had an important effect on the SSTs
306 of the Nordic Seas. By lowering the Greenland-Scotland ridge, introducing a subaerial Barents Sea,

307 and changes in river routing in North American and Europe in the HadCM3 model, Hill (2015)
308 found a stronger temperature anomaly in the northern Nordic Seas compared to previous model
309 setups, in which these differences had not been taken into account (Haywood & Valdes, 2004;
310 Haywood et al., 2013a). However, the simulated central Norwegian Sea SSTs are not strongly
311 affected by these changes in paleogeographic boundary conditions. Both the results from Hill (2015)
312 and the multi model mean SSTs from the Model Intercomparison Project (PlioMIP) (Haywood et
313 al., 2013a) are in line with the 2°C warmer Hole 642B SSTs that we present here. Thus, without
314 further tests, it is not shown that a deeper Greenland-Scotland ridge or a subaerial Barents Sea were
315 important in explaining the 2°C warmer SSTs at Hole 642B.

316 **5.3 Orbital scale mid-Piacenzian SST variability in the Norwegian Sea caused by changes in** 317 **insolation**

318 While the U_{37}^K SST record from Hole 642B does not show a long-term trend, temperature
319 variability of up to 4.2°C occurred at orbital time scales. This is greater than the Holocene
320 variability of 2.4°C within the Norwegian Sea (Calvo et al., 2002), yet insolation variability for
321 much of our record had a similar amplitude as during the Holocene. Furthermore, the amplitude of
322 the orbital scale temperature variability in the mid-Piacenzian is of comparable magnitude to the late
323 Pleistocene glacial-interglacial cycles in the Nordic Seas, but in the absence of feedbacks which
324 might be linked to the presence of large northern hemisphere ice sheets of the late Pleistocene. The
325 new Norwegian Sea SST data presented here demonstrates that consideration of only long-term
326 trends or averages hides the significant variability in Pliocene climate records. As Haywood et al.
327 (2013b) and Dowsett et al. (2013b) have proposed, an averaging of long-term proxy data results is
328 an inappropriate test for climate models which generally simulate shorter time windows. Because of
329 this, it is important to discuss the variability of the Norwegian Sea SSTs on the orbital time scale.

330 In the Hole 642B SST record, the cycles of cooling and warming are most pronounced between
331 3.264 and 3.21 Ma. Such orbital-scale variability is not as well-defined in the later part of the record
332 where the sample resolution is lower, although the SSTs remain variable. Both orbitally forced
333 insolation changes and the atmospheric content of CO₂ may influence these orbital scale climate
334 changes through their influence on radiative forcing. The IRD influx, while low, co-varies
335 significantly with SSTs.

336 **5.3.1 Origin and implications of Ice Rafted Debris**

337 Phases of increased IRD deposition at Hole 642B coincide with decreases in SST (Fig. 2a,b). Hence,
338 we infer that mobile ice occurred occasionally in the Norwegian Sea during the mid-Piacenzian, and
339 that a common forcing may have influenced both the IRD and SST variability. The mid-Piacenzian
340 influx of IRD to Hole 642B is low compared to that seen during fully glacial intervals of the
341 Pleistocene (Jansen et al., 2000). The land surrounding the Nordic Seas offers several possible
342 source of IRD. Small glacial buildup in the higher mountain ranges of western Scandinavia, and
343 icebergs drifting from Greenland, Iceland or Svalbard have been considered as such sources (Jansen
344 et al., 2000). We consider Scandinavia to be an unlikely source of IRD due to the warmer than
345 Holocene regional temperatures that would preclude glacial inception. This is supported by warmer
346 land temperatures during this time, based on a palynological reconstruction (Panitz et al., accepted).
347 Additionally, as model results have shown, the last glacial inception required temperatures 3°C
348 lower than modern (Born et al., 2010a). Thus the warmer temperatures of the Norwegian Sea and in
349 western Scandinavia make it unlikely that calving glaciers existed here. The lower topography of
350 western Norway during the Pliocene (Sohl et al., 2009) makes regional glaciation here less likely as
351 well. Jansen et al. (2000) suggested icebergs from Greenland and Iceland as possible IRD sources.
352 Svalbard and the subaerial Barents region are potential IRD sources as well. Icebergs originating

353 from these regions could be transported by the EGC, and further by eastward flowing branches of
354 the EGC north of Iceland, and could deposit low amounts of IRD at the outer Vøring Plateau. The
355 IRD identified in Hole 642B samples consist mainly of quartz grains and metamorphic rock
356 fragments, identified by their content of mica. Hence, the volcanic mineralogy of Iceland and the
357 sedimentary composition of Svalbard make them unlikely IRD source compared to the
358 metamorphic bedrock of Greenland. The potential of Greenland as a source region of icebergs is
359 supported by the IRD record at ODP Site 907 (Jansen et al., 2000), which shows several IRD peaks
360 that are contemporaneous with IRD peaks at Hole 642B, and that are orders of magnitude larger.
361 Site 907 is situated at the Iceland Plateau between Greenland and the Vøring Plateau (Fig. 1).
362 Furthermore, the continuous background IRD input to the Iceland Plateau implies that the Greenland
363 Ice Sheet had a calving margin throughout the investigated time interval. This supports results of ice
364 sheet models that indicate East Greenland as a likely site of early NHG (e.g. Lunt et al., 2008).
365 Therefore, we consider East Greenland to be the most likely source for the IRD deposited at Hole
366 642B during the mid-Piacenzian. While we consider other IRD sources to be less likely, their
367 contribution cannot be ruled out entirely. The potential connection of IRD transport from around the
368 Nordic Seas with SST variability in the Norwegian Sea suggests that the cause of the variability was
369 operating at a regional scale.

370 **5.3.2 Influence of atmospheric CO₂ concentration on SST variability**

371 Climate variability during the late Pleistocene glacials and interglacials has been strongly tied to
372 fluctuations in atmospheric CO₂. It is not clear how the atmospheric CO₂ concentration varied
373 through the mid-Piacenzian, with different studies giving largely different estimates (Badger et al.,
374 2013b; Martínez-Botí et al., 2015). The recent studies by Martínez-Botí et al. (2015) and Badger et
375 al. (2013) have high enough temporal resolution to resolve obliquity scale variability of atmospheric

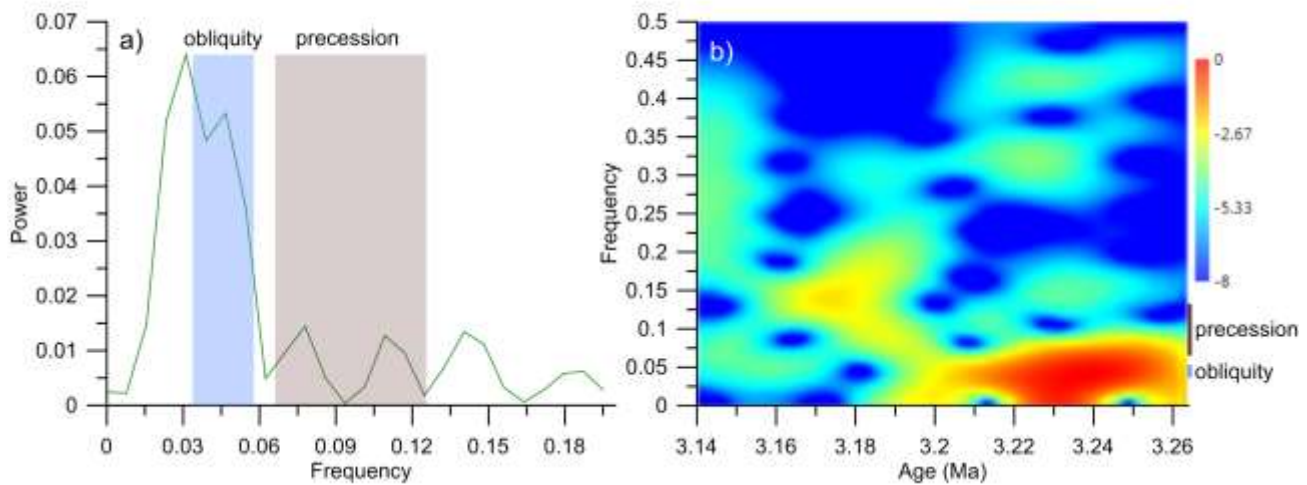
376 CO₂ (Fig. 2f). There is no clear correspondence between Hole 642B U^{K'}₃₇ SSTs and the atmospheric
377 CO₂ content as reconstructed by Martínez-Botí et al. (2015). Low CO₂ values do not coincide with
378 lower U^{K'}₃₇ SSTs (e.g. early MIS M1), and high CO₂ values do not correspond to high U^{K'}₃₇ SSTs
379 (e.g. late MIS M1) (Fig. 2b, f). In MIS KM6 the U^{K'}₃₇ SSTs and the CO₂ record show an opposite
380 development. While atmospheric CO₂ is an important factor for the globally warmer mid-Pliocene
381 (Haywood & Valdes, 2004) and the overall warmer U^{K'}₃₇ SSTs recorded in the Hole 642B (Section
382 5.2), no clear link can be established between U^{K'}₃₇ SST variability in the Norwegian Sea and the
383 variability in atmospheric CO₂ as reconstructed by Martínez-Botí et al (2015). This may in part be
384 due to uncertainties in both the age models and the proxies.

385 **5.3.3 Insolation and SST variability**

386 Summer insolation in the northern hemisphere had a strong effect on late Pleistocene and the
387 Holocene climate due to its interaction with ice sheets (Hays et al., 1976). Using a mathematical
388 calculation of past orbital parameters (Laskar et al., 2004), we compare the Hole 642B SST record
389 to summer insolation at 65°N (Fig. 2).

390 Relatively low insolation and low SSTs coincide during early KM6 and at the end of KM5,
391 however, low temperatures also occur during phases of higher insolation (e.g. late M1, KM3) and
392 high temperatures occur during phases of low insolation (e.g. early M1, late KM6). This inconsistent
393 relationship between temperature and summer insolation shows that there is no well-defined linear
394 relationship between Norwegian Sea SSTs and insolation during the mid-Piacenzian. This is in
395 contrast to observations from this area during the Holocene, when U^{K'}₃₇ SSTs develop in line with
396 the summer insolation at 65°N (Calvo et al., 2002; e.g. Risebrobakken et al., 2011).

397 Spectral analysis and evolutive spectra of the SST record (Fig. 3a,b) identify the dominance of
398 cyclicity in the range of obliquity in the early half of the record. This finding is in line with previous
399 studies proposing that the obliquity cycle was the dominant cycle for global climate variability
400 during the Pliocene (Lisiecki and Raymo, 2005). Around the 3.18 Ma cool event, the strength of
401 obliquity forcing is reduced, and cyclicity with a precession frequency emerges.



402

403 Figure 3: a) spectral analysis of SSTs (2ka interpolation), showing power of spectra (green line). The typical range of
404 frequencies of the obliquity cycle is marked by blue shading, the range of frequencies of the precession cycle is marked
405 by brown shading (based on Laskar et al., 2004); b) evolutionary spectra of SSTs (2ka interpolation). Colors indicate the
406 relative power. The brown bar on the right side indicates the range of frequencies of the precession cycle, the blue bar
407 indicates the range of the obliquity cycle. A size 32 Hanning window was applied. Calculations and the figure were
408 produced using the PAST3 software by Hammer et al. (2001).

409

410 It is notable that during the part of our records that shows strong obliquity-scale cyclicity, the
411 amplitude of insolation variability was similar that of the Holocene. This indicates that the
412 Norwegian Sea SST response to obliquity forcing was stronger during the mid-Piacenzian and
413 suggests that other forcings enhanced the impact on SST variability.

414 The predicted effect of obliquity is a strengthening (weakening) of seasonal contrasts during high
415 (low) obliquity (Berger, 1988). The 642B $U_{37}^{K'}$ SSTs shows several occurrences of possible SST
416 responses to changes in obliquity (Fig. 2). Cooling across the MIS M1/KM6 boundary and warming
417 out of MIS KM6 follow the obliquity trends, and the stability of the $U_{37}^{K'}$ SSTs during MIS KM5
418 occurs during an extended phase of low amplitude change in obliquity. However, the relationship is
419 complex, since after MIS KM5 low obliquity correlates with high SSTs during MIS KM4 and KM3
420 (Fig. 2). Although the evolutive spectra identify a shift towards precession-related SST variability
421 after 3.18 Ma (Fig. 3), it is difficult to isolate SST responses to this forcing in Figure 2, although
422 cool SSTs are found during low precession at 3.18 Ma and 3.14 Ma. The new data from Hole 642B
423 thus indicate that whilst there is a signature of orbital forcing in Norwegian Sea SSTs, the
424 relationship is complex and evolved through the mid-Piacenzian.

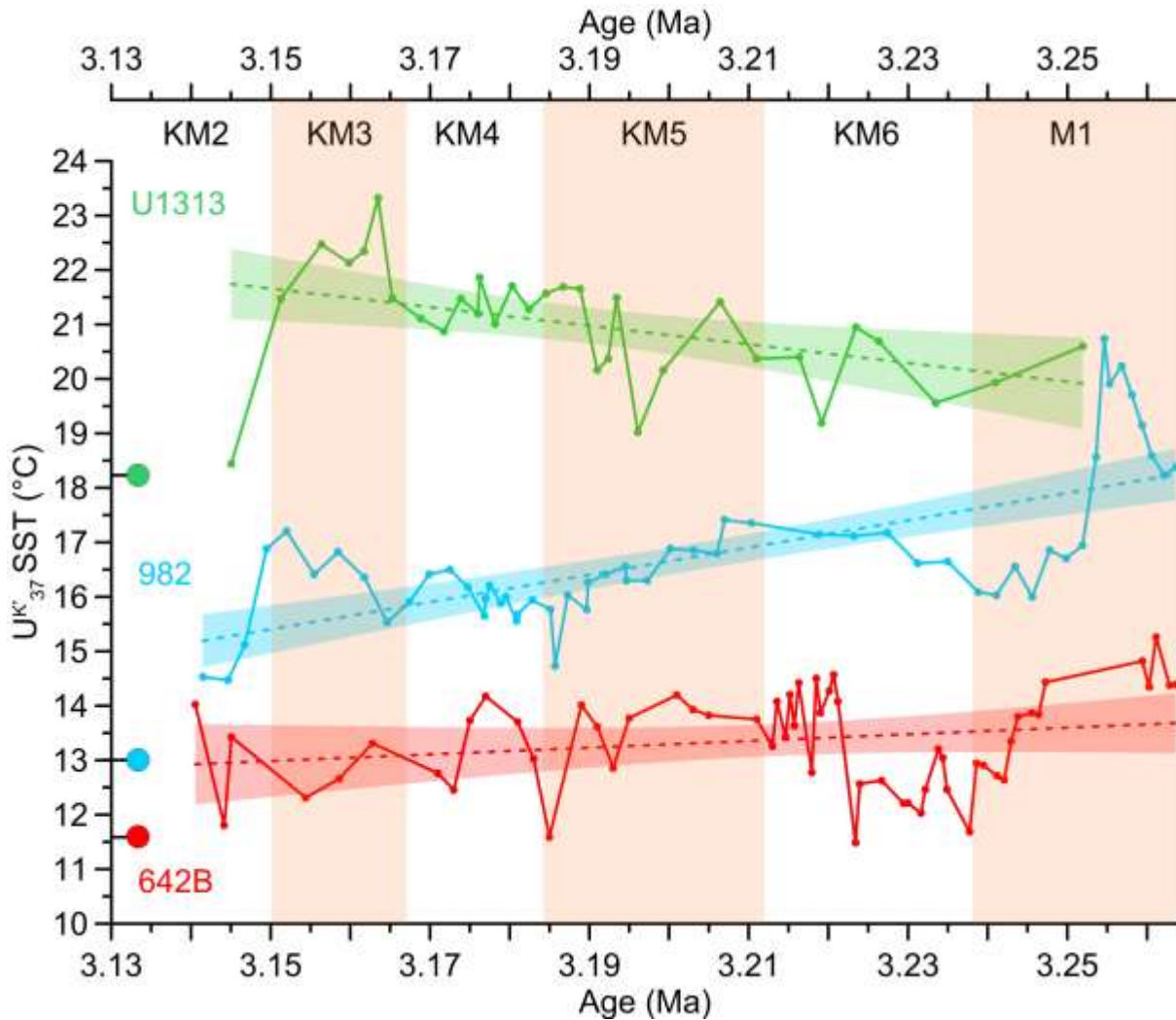
425

426 **5.4 Influence of the North Atlantic circulation on Norwegian Sea SST**

427 The transport of warm Atlantic water via the NAC is possibly an important factor in the temperature
428 development of the Norwegian Sea and may have left an imprint on the SSTs at Hole 642B. Since
429 the SST of the water masses transported into the Nordic Seas is affected by the subpolar gyre and
430 the subtropical gyre (e.g. Hátún et al., 2005), the contrast between North Atlantic and Norwegian
431 Sea could give some indication about the northward heat transport during the mid-Piacenzian and
432 whether this was notably different than during the Holocene. Several factors could account for a
433 changing temperature contrast between the North Atlantic and the Norwegian Sea: changes in heat
434 loss to the atmosphere, changes in the pathway of the warm NAC, changes in the mixing between
435 warmer water from Caribbean origin and the cooler water of the subtropical gyre. Here we will
436 focus on the question whether a stronger northward heat transport, as it has been proposed by

437 Raymo et al., (1996b) for the mid-Piacenzian Warm Period, is clearly supported by our data or not.
 438 If this was the case, it could be expressed in a warming both in the North Atlantic and in the
 439 Norwegian Sea, and thus a weak contrast.

440



441

442 **Figure 4:** U^K₃₇-based SST records and their linear trends (dashed lines) with 95% confidence intervals from (a) IODP
 443 Site U1313 (Naafs et al., 2010); (b) ODP Site 982 (Lawrence et al., 2009); (c) ODP Hole 642B. Dots on the temperature
 444 axis indicate core-top SSTs for U1313 (green, Naafs et al., 2010) and 982 (blue, Lawrence et al., 2009), and the
 445 Holocene average SST from Site MD95-2011 (red, Calvo et al., 2002). Orange vertical bars indicate MIS (from Lisiecki
 446 and Raymo, 2005).

447 Comparing the SST development at ODP Hole 642B with SST data from the North Atlantic shows
448 the meridional temperature gradient along the pathway of the NAC (Fig. 4). The high-resolution
449 SST records used for this comparison stem from ODP Site 982 (Lawrence et al., 2009), located on
450 the Rockall Plateau, and IODP Site U1313 (Naafs et al., 2010), on the upper western flank of the
451 Mid-Atlantic Ridge (Fig. 1). They are based on the $U_{37}^{K'}$ alkenone index, which makes them
452 comparable to the Hole 642B record presented here. Lawrence et al. (2009) assume a bias towards
453 summer SSTs in their data. Their SSTs are based on a different calibration than that of Naafs et al.
454 (2010) and our study, but the resulting difference is small ($<0.5^{\circ}\text{C}$) and does not impact the general
455 trends we discuss here. The SSTs at U1313 are interpreted by Naafs et al. (2010) as reflecting mean
456 annual temperatures, due to the close match of the core-top $U_{37}^{K'}$ SST with the modern annual mean
457 SST at the site. In this comparison of SST record we use the age models as they were published by
458 the respective authors. Because of the temporal uncertainties involved, any comparison on orbital
459 timescales should be treated with caution. However, the comparison of the long-term states and
460 trends seen in these records during the mid-Piacenzian is more robust in this regard.

461 As shown in sections 5.2 and 5.3, SSTs at Hole 642B are ca. 2°C warmer than the Holocene average
462 over the whole 3.164-3.140 Ma time window, with orbital scale variability. The record of Site 982
463 shows an early warming and a distinct cooling during MIS M1, after which this record shows stable
464 SSTs, until another cooling takes place during MIS KM2. This relative stability between the latter
465 half of MIS M1 and MIS KM3 is comparable to the development of SSTs at Hole 642B. The
466 cooling seen within MIS M1 and during KM2 in the Site 982 SST record is potentially related to
467 eastward shifts or extension of the subpolar gyre. Lawrence et al. (2009) suggested that such
468 variability of the subpolar gyre could explain the generally high SST variability in the longer
469 Pliocene record from this site and that orbital scale variability seen could reflect climatic instability

470 associated with ice sheet growth and shifting wind systems of the northern hemisphere. This could
471 be expressed through changes in the subpolar gyre.

472 The Site U1313 record shows a warming trend from MIS M1 to early MIS KM3. A northward shift
473 and strengthening of the subtropical gyre in the mid-Piacenzian, compared to its late Holocene state,
474 has been proposed by Lutz (2011), through a comparison of foraminiferal assemblages. If this shift
475 in the subtropical gyre progressed throughout our study interval, it would explain the warming trend
476 at U1313. Hence, the differences in the SST development at Site 982 and Site U1313 could be
477 explained by positional shifts in the subpolar gyre and the subtropical gyre.

478 The fact that the SST trend at Hole 642B is more similar to that at Site 982 than that at Site U1313
479 (Fig. 4) suggests that the state of the subpolar gyre had a stronger impact on the Nordic Seas than
480 the subtropical gyre. This has been established for the modern climate on a decadal time scale by
481 Hátún et al. (2005) and may have been a long-term feature of mid-Piacenzian climate.

482 However, a weakening of the subpolar gyre due to southward shifts of the Polar and Arctic Fronts
483 was suggested to be an important factor in the transition towards a stronger glacial climate during
484 the last glacial inception (Mokeddem et al., 2014). In this scenario, a vigorous and relatively warm
485 subpolar gyre is indicative of a Holocene-like climate state, where mixing of subpolar and
486 subtropical water masses produces the SST and salinity signature of the Atlantic Water flowing into
487 the Norwegian Sea (Hátún et al., 2005). Setting out from this Holocene-like state, a weakening of
488 the subpolar gyre would boost the warming influence of the NAC on the Norwegian Sea. Because
489 the warmth of the Norwegian Sea is near the global average warmth of the mid-Piacenzian, and
490 there is no indication of a warming trend in the Norwegian Sea comparable to that of Site U1313, it

491 is possible that the presence of a strong subpolar gyre constrained the warmer inflow of the NAC
492 into the Norwegian Sea.

493 The meridional gradient between Hole 642B and North Atlantic sites gives no indication that the
494 oceanographic regime of the mid-Piacenzian was drastically different from that of the Holocene: the
495 subpolar gyre and the mixing of water south of Iceland was comparable, and the NAC did not have a
496 stronger impact on warm surface water being transported into the Nordic Seas. The warmer than
497 Holocene average temperatures are explained by the globally warmer climate state of the Pliocene
498 as modelled by Haywood and Valdes (2004) and reconstructed in proxy studies (Dowsett et al.,
499 2013a). While we do not discuss orbital scale variability in the records due to uncertainties in the
500 matching of the respective age models, it is clear that all three records vary on orbital time scales.
501 The respective SST trends of the records are robust in regard to orbital scale shifts of their age
502 models. Based on these new data from the Norwegian Sea, it appears that the mid-Piacenzian
503 northward heat transport was not significantly increased compared to its average Holocene state, in
504 agreement with model simulations discussed by Zhang et al. (2013).

505 The divergent SST trends at the sites we compare suggest changing relationships between the
506 subpolar gyre, the subtropical gyre and the Norwegian Sea over time. These relationships are likely
507 dependent on the overall climate state of the region. One major question is whether the Greenland
508 ice sheet is a factor in linking the Nordic Seas and the subpolar gyre together. The EGC, and
509 consequently the strong east-west gradients of the Nordic Seas, was established in its modern pattern
510 by 4.5 Ma (Schepper et al., 2015), and the arctic summer sea ice cover was present at the Yermak
511 Plateau from 4 Ma (Knies et al., 2014b). Born et al. (2010b) show a link between increased
512 freshwater transport by the EGC and a weakening of the SPG. If the state of Northern Hemisphere
513 Glaciation affected the SSTs at Site 982, as suggested by Lawrence et al. (2009) for the late

514 Pliocene, the expanded SPG of the mid-Piacenzian could be due to relatively low amounts of
515 freshwater inflow from the Nordic Seas. If the strengthening of NHG during the late Pliocene is
516 comparable to the last glacial inception, which Mokeddem et al. (2014) linked to a weakening of the
517 subpolar gyre and a stronger influence of the warm NAC on the Nordic Seas, this transition should
518 be marked by occurrences of relatively warm SSTs in the Norwegian Sea. This would also be
519 reflected in a strengthening of the latitudinal contrast between the warm Norwegian Sea and the
520 western reaches of the Nordic Seas, close to the cooling influence of the Greenland ice sheet and the
521 EGC.

522

523 **6. Conclusions**

524 The SST evolution of the Norwegian Sea during the mid-Piacenzian has been documented in
525 unprecedented detail. We conclude that:

- 526 • The SST of the Norwegian Sea during mid-Piacenzian was on average 2-3°C warmer than
527 during the Holocene. This is in line with modelled mid-Piacenzian Norwegian Sea SSTs and
528 represents a smaller anomaly than seen in previous proxy records from the Nordic Seas.
- 529 • Variability of SSTs on orbital time scales can be distinguished in the Norwegian Sea during
530 the time interval 3.264-3.14 Ma. Spectral analysis shows cyclicity predominantly on the
531 obliquity time scale. The correlation of IRD from the Nordic Seas region and SSTs shows
532 the influence of obliquity and precession on the Norwegian Sea SSTs, and that these forcings
533 were also influencing the variability of ice rafting.
- 534 • Our data are in agreement with existing model simulations of Pliocene climate. This is true
535 both for those simulations that include a near-modern paleogeography and a more recent one

536 that includes specific Pliocene paleogeography. This suggests that the Norwegian Sea was
537 not strongly affected by changes in these particular boundary conditions.

- 538 • The position or eastward extent of the subpolar gyre influences the Norwegian Sea SST
539 development to a larger degree than the warmer NAC. This suggests the existence of a
540 strong subpolar gyre, similar to the Holocene setting, and gives no indication of a stronger
541 influence of the NAC on warm surface water transport into the Nordic Seas.

542

543 **Acknowledgements**

544 We thank the Norwegian Research Council for funding project No. 221712, Ocean Controls on
545 high-latitude climate sensitivity - a Pliocene case study (OCCP). BR has received additional funding
546 through the Earth System Modeling (Statoil) and DYNAWARM (Centre for Climate Dynamics at the
547 Bjerknes Centre) project. We gratefully acknowledge the indispensable work done by the Ocean
548 Drilling Project in acquiring the deep sea sediments used in this study. We thank Eystein Jansen and
549 Sina Panitz for valuable discussion and improvements to the manuscript. We thank Juliane Müller,
550 Amanda Hayton and Martin West for technical assistance and advice in the laboratory. Thanks are
551 also due to David Naafs and two anonymous reviewers for their comments and corrections which
552 helped to improve the quality of this paper. The new datasets discussed in this paper are available at
553 <https://doi.pangaea.de/10.1594/PANGAEA.858944>.

554 **References**

- 555 Andruleit, H.A., 1997. Coccolithophore fluxes in the Norwegian-Greenland Sea: Seasonality and
556 assemblage alterations. *Mar. Micropaleontol.* 31, 45–64. doi:10.1016/S0377-8398(96)00055-2
- 557 Badger, M.P.S., Schmidt, D.N., Mackensen, A., Pancost, R.D., 2013. High-resolution alkenone
558 palaeobarometry indicates relatively stable pCO₂ during the Pliocene (3.3-2.8 Ma). *Philos.*
559 *Trans. A. Math. Phys. Eng. Sci.* 371, 20130094. doi:10.1098/rsta.2013.0094
- 560 Berger, A.L., 1988. Milankovitch Theory and Climate. *Geophysique* 26, 624–657.
561 doi:10.1029/RG026i004p00624
- 562 Blindheim, J., Østerhus, S., 2005. The Nordic Seas, Main Oceanographic Features. *Geophys.*
563 *Monogr. Ser.* 158, 11–37. doi:10.1029/158GM03
- 564 Born, A., Kageyama, M., Nisancioglu, K.H., 2010a. Warm Nordic Seas delayed glacial inception in
565 Scandinavia. *Clim. Past* 6, 817–826. doi:10.5194/cp-6-817-2010
- 566 Born, A., Nisancioglu, K.H., Braconnot, P., 2010b. Sea ice induced changes in ocean circulation
567 during the Eemian. *Clim. Dyn.* 35, 1361–1371. doi:10.1007/s00382-009-0709-2
- 568 Boyer, T.P., Antonov, J.I., Baranova, O.K., Coleman, C., Garcia, H.E., Grodsky, A., Johnson, D.R.,
569 Locarnini, R.A., Mishonov, A. V., O'Brien, T.D., Paver, C.R., Reagan, J.R., Seidov, D.,
570 Smolyar, I. V., Zweng, M.M., Levitus, S., 2013. The World Ocean Database.
571 doi:10.2481/dsj.WDS-041
- 572 Calvo, E., Grimalt, J.O., Jansen, E., 2002. High resolution UK37 sea surface temperature
573 reconstruction in the Norwegian Sea during the Holocene. *Quat. Sci. Rev.* 21, 1385–1394.
574 doi:10.1016/S0277-3791(01)00096-8
- 575 De Schepper, S., Groeneveld, J., Naafs, B.D.A., Van Renterghem, C., Hennissen, J.A.I., Head, M.J.,

- 576 Louwye, S., Fabian, K., 2013. Northern Hemisphere Glaciation during the Globally Warm
577 Early Late Pliocene. *PLoS One* 8, e81508.
- 578 Dowsett, H.J., Foley, K.M., Stoll, D.K., Chandler, M.A., Sohl, L.E., Bentsen, M., Otto-Bliesner,
579 B.L., Bragg, F.J., Chan, W.-L., Contoux, C., Dolan, A.M., Haywood, A.M., Jonas, J.A., Jost,
580 A., Kamae, Y., Lohmann, G., Lunt, D.J., Nisancioglu, K.H., Abe-Ouchi, A., Ramstein, G.,
581 Riesselman, C.R., Robinson, M.M., Rosenbloom, N.A., Salzmann, U., Stepanek, C., Strother,
582 S.L., Ueda, H., Yan, Q., Zhang, Z., 2013a. Sea surface temperature of the mid-Piacenzian
583 ocean: a data-model comparison. *Nat. Sci. Reports* 3, 2013. doi:10.1038/srep02013
- 584 Dowsett, H.J., Robinson, M.M., Haywood, A.M., Salzmann, U., Hill, D.J., Sohl, L.E., Chandler,
585 M.A., Williams, M., Foley, K.M., Stoll, D.K., 2010. The PRISM3D paleoenvironmental
586 reconstruction. *Stratigraphy* 7, 123–139.
- 587 Dowsett, H.J., Robinson, M.M., Stoll, D.K., Foley, K.M., Johnson, A.L.A., Williams, M.,
588 Riesselman, C.R., 2013b. The PRISM (Pliocene palaeoclimate) reconstruction: time for a
589 paradigm shift. *Philos. Trans. A. Math. Phys. Eng. Sci.* 371, 20120524.
590 doi:10.1098/rsta.2012.0524
- 591 Hammer, Ø., Harper, D.A.T., Ryan, P.D., 2001. PAST: Paleontological Statistics Software Package
592 for Education and Data Analysis. v.2.17. *Palaeontol. Electron.* 4(1): 9pp.
- 593 Hansen, B., Østerhus, S., 2000. North Atlantic–Nordic Seas exchanges. *Prog. Oceanogr.* 45, 109–
594 208. doi:10.1016/S0079-6611(99)00052-X
- 595 Hátún, H., Sandø, A.B., Drange, H., Hansen, B., Valdimarsson, H., 2005. Influence of the Atlantic
596 subpolar gyre on the thermohaline circulation. *Science* (80-.). 309, 1841–1844.
597 doi:10.1126/science.1114777
- 598 Haug, G.H., Tiedemann, R., 1998. Effect of the formation of the Isthmus of Panama on Atlantic

599 Ocean thermohaline circulation. *Nature* 393, 673–676. doi:10.1038/31447

600 Hays, J.D., Imbrie, J., Shackleton, N.J., 1976. Variations in the Earth's Orbit: Pacemaker of the Ice
601 Ages. *Science* (80-.). 194, 1121–1132. doi:10.1126/science.194.4270.1121

602 Haywood, A.M., Dolan, A.M., Pickering, S.J., Dowsett, H.J., McClymont, E.L., Prescott, C.L.,
603 Salzmann, U., Hill, D.J., Hunter, S.J., Lunt, D.J., Pope, J.O., Valdes, P.J., 2013. On the
604 identification of a Pliocene time slice for data-model comparison. *Philos. Trans. A. Math. Phys.*
605 *Eng. Sci.* 371, 20120515. doi:10.1098/rsta.2012.0515

606 Haywood, A.M., Dowsett, H.J., Dolan, A.M., Rowley, D., Abe-Ouchi, A., Otto-Bliesner, B.,
607 Chandler, M.A., Hunter, S.J., Lunt, D.J., Pound, M., Salzmann, U., 2015. Pliocene Model
608 Intercomparison (PliMIP) Phase 2: scientific objectives and experimental design. *Clim. Past*
609 *Discuss.* 11, 4003–4038. doi:10.5194/cpd-11-4003-2015

610 Haywood, A.M., Hill, D.J., Dolan, A.M., Otto-Bliesner, B.L., Bragg, F.J., Chan, W.L., Chandler,
611 M.A., Contoux, C., Dowsett, H.J., Jost, A., Kamae, Y., Lohmann, G., Lunt, D.J., Abe-Ouchi,
612 A., Pickering, S.J., Ramstein, G., Rosenbloom, N.A., Salzmann, U., Sohl, L., Stepanek, C.,
613 Ueda, H., Yan, Q., Zhang, Z., Huber, M., 2013. Large-scale features of Pliocene climate:
614 Results from the Pliocene Model Intercomparison Project. *Clim. Past* 9, 191–209.
615 doi:10.5194/cp-9-191-2013

616 Haywood, A.M., Valdes, P.J., 2004. Modelling Pliocene warmth: contribution of atmosphere,
617 oceans and cryosphere. *Earth Planet. Sci. Lett.* 218, 363–377. doi:10.1016/S0012-
618 821X(03)00685-X

619 Hill, D.J., 2015. The non-analogue nature of Pliocene temperature gradients. *Earth Planet. Sci. Lett.*
620 425, 232–241. doi:10.1016/j.epsl.2015.05.044

621 Indermühle, A., Stocker, T.F., Joos, F., Fischer, H., Smith, H.J., Wahlen, M., Deck, B., Mastroianni,

622 D., Tschumi, J., Blunier, T., Meyer, R., Stauffer, B., 1999. Holocene carbon-cycle dynamics
623 based on CO₂ trapped in ice at Taylor Dome, Antarctica. *Nature* 398, 121–126.
624 doi:10.1038/18158

625 Jansen, E., Fronval, T., Rack, F., Channell, J.E.T., 2000. Pliocene-Pleistocene ice rafting history and
626 cyclicity in the Nordic Seas during the last 3.5 Myr. *Paleoceanography* 15, 709–721.
627 doi:10.1029/1999PA000435

628 Jansen, E., Sjøholm, J., 1991. Reconstruction of glaciation over the past 6 Myr from ice-borne
629 deposits in the Norwegian Sea. *Nature* 349, 600–603. doi:10.1038/349600a0

630 Khodri, M., Cane, M.A., Kukla, G.J., Gavin, J., Braconnot, P., 2005. The impact of precession
631 changes on the Arctic climate during the last interglacial-glacial transition. *Earth Planet. Sci.*
632 *Lett.* 236, 285–304. doi:10.1016/j.epsl.2005.05.011

633 Kleiven, H.F., Jansen, E., Fronval, T., Smith, T.M., 2002. Intensification of Northern Hemisphere
634 glaciations in the circum Atlantic region (3.5-2.4 Ma) - ice-rafted detritus evidence.
635 *Palaeogeogr. Palaeoclimatol. Palaeoecol.* 184, 213–223.

636 Knies, J., Cabedo-Sanz, P., Belt, S.T., Baranwal, S., Fietz, S., Rosell-Melé, A., 2014. The
637 emergence of modern sea ice cover in the Arctic Ocean. *Nat. Commun.* 5, 5608.
638 doi:10.1038/ncomms6608

639 Kornilova, O., Rosell-Melé, A., 2003. Application of microwave-assisted extraction to the analysis
640 of biomarker climate proxies in marine sediments. *Org. Geochem.* 34, 1517–1523.
641 doi:10.1016/S0146-6380(03)00155-4

642 Laskar, J., Robutel, P., Joutel, F., Gastineau, M., Correia, A.C.M., Levrard, B., 2004. A long-term
643 numerical solution for the insolation quantities of the Earth. *Astron. Astrophys.* 428, 261–285.
644 doi:10.1051/0004-6361:20041335

- 645 Lawrence, K.T., Herbert, T.D., Brown, C.M., Raymo, M.E., Haywood, A.M., 2009. High-amplitude
646 variations in North Atlantic sea surface temperature during the early Pliocene warm period.
647 *Paleoceanography* 24. doi:10.1029/2008PA001669
- 648 Lisiecki, L.E., Raymo, M.E., 2005. A Pliocene-Pleistocene stack of 57 globally distributed benthic
649 $\delta^{18}\text{O}$ records. *Paleoceanography* 20. doi:10.1029/2004PA001071
- 650 Lunt, D.J., Foster, G.L., Haywood, A.M., Stone, E.J., 2008. Late Pliocene Greenland glaciation
651 controlled by a decline in atmospheric CO₂ levels. *Nature* 454, 1102–5.
652 doi:10.1038/nature07223
- 653 Lutz, B.P., 2011. Shifts in North Atlantic planktic foraminifer biogeography and subtropical gyre
654 circulation during the mid-Piacenzian warm period. *Mar. Micropaleontol.* 80, 125–149.
655 doi:10.1016/j.marmicro.2011.06.006
- 656 Martínez-Botí, M.A., Foster, G.L., Chalk, T.B., Rohling, E.J., Sexton, P.F., Lunt, D.J., Pancost,
657 R.D., Badger, M.P.S., Schmidt, D.N., 2015. Plio-Pleistocene climate sensitivity evaluated using
658 high-resolution CO₂ records. *Nature* 518, 49–54. doi:10.1038/nature14145
- 659 Maslin, M.A., Li, X.S., Loutre, M.-F., Berger, A.L., 1998. The contribution of orbital forcing to the
660 progressive intensification of Northern Hemisphere glaciation. *Quat. Sci. Rev.* 17, 411–426.
661 doi:10.1016/S0277-3791(97)00047-4
- 662 Miller, G.H., Alley, R.B., Brigham-Grette, J., Fitzpatrick, J.J., Polyak, L., Serreze, M.C., White,
663 J.W.C., 2010. Arctic amplification: can the past constrain the future? *Quat. Sci. Rev.* 29, 1779–
664 1790. doi:10.1016/j.quascirev.2010.02.008
- 665 Mokeddem, Z., McManus, J.F., Oppo, D.W., 2014. Oceanographic dynamics and the end of the last
666 interglacial in the subpolar North Atlantic. *Proc. Natl. Acad. Sci. U. S. A.* 111, 11263–8.
667 doi:10.1073/pnas.1322103111

668 Moros, M., Emeis, K.C., Risebrobakken, B., Snowball, I., Kuijpers, A., McManus, J.F., Jansen, E.,
669 2004. Sea surface temperatures and ice rafting in the Holocene North Atlantic: climate
670 influences on northern Europe and Greenland. *Quat. Sci. Rev.* 23, 2113–2126.
671 doi:10.1016/j.quascirev.2004.08.003

672 Mudelsee, M., Raymo, M.E., 2005. Slow dynamics of the Northern Hemisphere glaciation.
673 *Paleoceanography* 20. doi:10.1029/2005PA001153

674 Müller, P.J., Kirst, G., Ruhland, G., von Storch, I., Rosell-Melé, A., 1998. Calibration of the
675 alkenone paleotemperature index UK'37 based on core-tops from the eastern South Atlantic
676 and the global ocean (60 N-60 S). *Geochim. Cosmochim. Acta* 62, 1757–1772.
677 doi:10.1016/S0016-7037(98)00097-0

678 Naafs, B.D.A., Hefter, J., Acton, G., Haug, G.H., Martínez-García, A., Pancost, R.D., Stein, R.,
679 2012. Strengthening of North American dust sources during the late Pliocene (2.7Ma). *Earth
680 Planet. Sci. Lett.* 317-318, 8–19. doi:10.1016/j.epsl.2011.11.026

681 Naafs, B.D.A., Stein, R., Hefter, J., Khélifi, N., De Schepper, S., Haug, G.H., 2010. Late Pliocene
682 changes in the North Atlantic Current. *Earth Planet. Sci. Lett.* 298, 434–442.
683 doi:10.1016/j.epsl.2010.08.023

684 Panitz, S., Salzmann, U., Risebrobakken, B., De Schepper, S., Pound, M.J., accepted. Climate
685 variability and long-term expansion of peat lands in Arctic Norway during the late Pliocene
686 (ODP Site 642, Norwegian Sea). *Clim. Past.*

687 Prah, F.G., Wakeham, S.G., 1987. Calibration of unsaturation patterns in long-chain ketone
688 compositions for palaeotemperature assessment. *Nature* 330, 367–369. doi:10.1038/330367a0

689 Prescott, C.L., Haywood, A.M., Dolan, A.M., Hunter, S.J., Pope, J.O., Pickering, S.J., 2014.
690 Assessing orbitally-forced interglacial climate variability during the mid-Pliocene Warm

691 Period. Earth Planet. Sci. Lett. 400, 261–271. doi:10.1016/j.epsl.2014.05.030

692 Raymo, M.E., Grant, B., Horowitz, M., Rau, G.H., 1996. Mid-Pliocene warmth: stronger
693 greenhouse and stronger conveyor. *Mar. Micropaleontol.* 27, 313–326.

694 Risebrobakken, B., Dokken, T., Smedsrud, L.H., Andersson, C., Jansen, E., Moros, M., Ivanova, E.
695 V., 2011. Early Holocene temperature variability in the Nordic Seas: The role of oceanic heat
696 advection versus changes in orbital forcing. *Paleoceanography* 26. doi:10.1029/2011PA002117

697 Risebrobakken, B., Moros, M., Ivanova, E. V., Chistyakova, N., Rosenberg, R., 2010. Climate and
698 oceanographic variability in the SW Barents Sea during the Holocene. *The Holocene* 20, 609–
699 621. doi:10.1177/0959683609356586

700 Risebrobakken, B., Andersson, C., De Schepper, S., McClymont, E., in review. High-amplitude, low
701 frequency Pliocene climate variability – identifying climate phases and transitions in the eastern
702 Nordic Seas. *Paleoceanography*.

703 Robinson, M.M., 2009. New quantitative evidence of extreme warmth in the Pliocene Arctic.
704 *Stratigraphy* 6, 265–275.

705 Schepper, S. De, Schreck, M., Beck, K.M., Matthiessen, J., 2015. Early Pliocene onset of modern
706 Nordic Seas circulation due to ocean gateway changes. *Nat. Commun.* 6, 1–8.
707 doi:10.1038/ncomms9659

708 Schlitzer, R., 2015. Ocean Data View, <http://odv.awi.de>.

709 Schreck, M., Meheust, M., Stein, R., Matthiessen, J., 2013. Response of marine palynomorphs to
710 Neogene climate cooling in the Iceland Sea (ODP Hole 907A). *Mar. Micropaleontol.* 101, 49–
711 67. doi:10.1016/j.marmicro.2013.03.003

712 Sohl, L.E., Chandler, M.A., Schmunk, R.B., Mankoff, K., Jeffrey, A., Dowsett, H.J., 2009.

713 PRISM3/GISS topographic reconstruction. U.S. Geol. Surv. Data Ser. 419.

714 Stocker, T.F., Qin, D., Plattner, G.-K., Tignor, M., Allen, S.K., Boschung, J., Nauels, A., Xia, Y.,
715 Bex, V., Midgley, P.M., 2013. The Physical Science Basis. Contribution of Working Group I to
716 the Fifth Assessment Report of the Intergovernmental Panel on Climate Change. Ipcc 1552.
717 doi:10.1017/CBO9781107415324.Summary

718 Zhang, Z., Nisancioglu, K.H., Ninnemann, U.S., 2013. Increased ventilation of Antarctic deep water
719 during the warm mid-Pliocene. Nat. Commun. 4, 1499. doi:10.1038/ncomms2521

720